The Astrophysical Journal, 979:222 (10pp), 2025 February 1 https://doi.org/10.3847/1538-4357/ada891

PUI Heating in the Supersonic Solar Wind

Parisa Mostafavi[1], Laxman Adhikari[2], Bishwas L. Shrestha[3], Gary P. Zank[2,4], Merav Opher[5], Matthew E. Hill[1], Heather A. Elliott[6], Pontus C. Brandt[1], Ralph L. McNutt[1], David J. McComas[3], Andrew R. Poppe[7], Elena Provornikova[1], Romina Nikoukar[1], Peter Kollmann[1], S. Alan Stern[8], Kelsi N. Singer[8], Anne Verbiscer[9,10], and Joel Parker[8]

[1] Johns Hopkins Applied Physics Laboratory, Laurel, MD 20723, USA; parisa.mostafavi@jhuapl.edu
[2] Department of Space Science, University of Alabama in Huntsville, Huntsville, AL 35899, USA
[3] Department of Astrophysical Sciences, Princeton University, Princeton, NJ 08544, USA
[4] Center for Space Plasma and Aeronomic Research (CSPAR), University of Alabama in Huntsville, Huntsville, AL 35899, USA
[5] Astronomy Department, Boston University, Boston, MA, USA
[6] Southwest Research Institute, San Antonio, TX, USA
[7] University of California Berkeley, Berkeley, CA, USA
[8] Southwest Research Institute, Boulder, CO, USA
[9] Space Sciences Laboratory, University of California, Berkeley, CA 94720, USA
[10] Department of Astronomy, University of Virginia, Charlottesville, VA, USA
Received 2024 October 7; revised 2024 November 22; accepted 2025 January 6; published 2025 January 29

Abstract

The outer heliosphere is profoundly influenced by nonthermal energetic pickup ions (PUIs), which dominate the internal pressure of the solar wind beyond ~10 au, surpassing both solar wind and magnetic pressures. PUIs are formed mostly through charge exchange between interstellar neutral atoms and solar wind ions. This study examines the apparent heating of PUIs in the distant supersonic solar wind before reaching the heliospheric termination shock. New Horizons' SWAP observations reveal an unexpected PUI temperature change between 2015 and 2020, with a notable bump in PUI temperature. Concurrent observations from the ACE and Wind spacecraft at 1 au indicate a ~50% increase in solar wind dynamic pressure at the end of 2014. Our simulation suggests that the bump observed in the PUI temperature by New Horizons is largely associated with the enhanced solar wind dynamic pressure observed at 1 au. Additional PUI temperature enhancements imply the involvement of other heating mechanisms. Analysis of New Horizons data reveals a correlation between shocks and PUI heating during the declining phase of the solar cycle. Using a PUI-mediated plasma model, we explore shock structures and PUI heating, finding that shocks preferentially heat PUIs over the thermal solar wind in the outer heliosphere. We also show that the broad shock thickness observed by New Horizons is due to the large diffusion coefficient associated with PUIs. Shocks and compression regions in the distant supersonic solar wind lead to elevated PUI temperatures and thus they can increase the production of energetic neutral atoms with large energy.

Unified Astronomy Thesaurus concepts: Heliosphere (711); Pickup ions (1239); Shocks (2086); Solar wind (1534)

1. Introduction

The outer heliosphere, extending from approximately the region beyond the ionization cavity to the heliopause, remains a poorly understood and highly dynamic region. This region is influenced by energetic nonthermal pickup ions (PUIs), which originate mostly from charge exchange between interstellar neutral atoms and thermal solar wind ions within the heliosphere (C. L. Semar 1970). The study of PUIs is crucial for understanding various phenomena in the outer heliosphere, as emphasized by G. P. Zank et al. (1996b) in their work on PUIs. These particles play a significant role in the transport of energy, momentum, and mass throughout the heliosphere. PUIs constitute the primary internal pressure within the outer heliosphere, surpassing the thermal pressure of the solar wind particles and the magnetic pressure (L. F. Burlaga et al. 1996; G. P. Zank 2014; D. J. McComas et al. 2017).

The dominant source of PUIs near 1 au is attributed to interstellar He atoms, which possess a high ionization potential and are capable of propagating closer to the Sun before undergoing ionization to become He^+ PUIs (W. I. Axford 1972; G. L. Siscoe & N. R. Mukherjee 1972). On the other hand, H^+ (proton) PUIs become an important component in the outer regions, beyond a few au from the Sun, defined by the size of the hydrogen ionization cavity (D. J. McComas et al. 2017; J. M. Sokół et al. 2019). The presence of interstellar proton PUIs was initially confirmed through observations by Ulysses, which detected these particles at distances of up to approximately 5 au from the Sun (G. Gloeckler et al. 1993). Although Voyager 1 and 2 are not specifically designed for direct measurements of nonthermal PUIs, they have played a crucial role in indirectly detecting these particles. For instance, several studies have effectively identified the presence of PUIs in the outer heliosphere by monitoring the wave excitation resulting from their creation (S. J. Hollick et al. 2018a, 2018b).

The New Horizons spacecraft stands as the sole platform capable of conducting in situ and direct measurements of interstellar PUIs within the outer heliosphere, particularly beyond 5 au (S. A. Stern 2008). Researchers have leveraged data from New Horizons to gain valuable insights into the outer heliosphere, and more specifically, the characteristics of PUIs (D. McComas et al. 2008; D. J. McComas et al. 2017; G. P. Zank et al. 2018; E. J. Zirnstein et al. 2018b; P. Kollmann et al. 2019; D. J. McComas et al. 2021, 2022; B. L. Shrestha

et al. 2023). On board the New Horizons spacecraft, two specialized instruments are dedicated to the precise measurement of PUIs: the Solar Wind Around Pluto (SWAP) instrument and the Pluto Energetic Particle Spectrometer Science Investigation (PEPSSI) instrument. The SWAP instrument focuses on measuring the core of the thermal solar wind and interstellar H^+ PUIs, as detailed by D. McComas et al. (2008). The PEPSSI instrument is proficient at measuring interstellar He^+ PUIs and higher energy particles (R. L. McNutt et al. 2008).

The distribution of nonthermal PUIs exhibits a notable cutoff at approximately twice the solar wind speed in the rest frame (V. M. Vasyliunas & G. L. Siscoe 1976). These particles typically possess an energy of around 1 keV upon their formation (see, e.g., G. P. Zank et al. 1996b). It is assumed that PUIs are decelerated as they propagate in the heliosphere due to adiabatic deceleration under conditions of the radial expansion of a constant speed solar wind (V. M. Vasyliunas & G. L. Siscoe 1976). Notably, they can undergo acceleration processes, resulting in their energization to higher energy levels (G. P. Zank et al. 1996b, 2010; R. Kumar et al. 2018; J. M. Sokół et al. 2022). Multiple prior investigations have provided evidence that PUIs significantly enhance their energy during the crossing of the heliospheric termination shock (HTS; G. P. Zank et al. 1996b, 2010; B. Zieger et al. 2015; P. Mostafavi et al. 2017a, 2018; J. Giacalone et al. 2021; J. D. Richardson et al. 2022; M. Kornbleuth et al. 2023). Remarkably, they exhibit a preference for heating at the HTS, where they acquire the majority of their additional energy. Meanwhile, the thermal solar wind plasma component continues downstream of the HTS without experiencing significant heating (G. P. Zank et al. 1996b, 2010; J. D. Richardson 2008; P. Mostafavi et al. 2017a, 2018).

Moreover, PUIs can be further heated in the inner heliosheath (IHS), the region between the HTS and the heliopause, from various mechanisms. For instance, some recent studies showed that turbulence within the IHS may further heat the PUIs after crossing the HTS (L. A. Fisk & G. Gloeckler 2017; G. P. Zank et al. 2018, 2021; B. Zieger et al. 2020). Turbulent fluctuations can transfer energy from large to small scales, initiating a cascade of energy that can ultimately heat the solar wind and possibly PUIs (G. P. Zank et al. 1996a, 2017, 2018; L. Adhikari et al. 2017, 2021; P. A. Isenberg et al. 2023). P. Mostafavi et al. (2019) proposed that another mechanism such as the presence of shocks in the IHS results in greater heating of the PUI component since IHS shocks preferentially heat the PUIs and not the thermal solar wind. Another process, magnetic reconnection, can occur within the IHS (J. F. Drake et al. 2010; M. Opher et al. 2011), which can contribute additional heating to PUIs. For instance, evidence of magnetic reconnection within the IHS has been observed through Voyager 2 observations, where magnetic islands accompanied by energetic particles were detected (G. P. Zank et al. 2015; L. L. Zhao et al. 2019). Simulations have shown that a Rayleigh–Taylor–like instability can mix heliospheric and interstellar plasmas, leading to the formation of turbulent heliospheric jets and further heating of PUIs (G. P. Zank 1999; V. Florinski et al. 2005; M. Opher et al. 2015, 2021).

As they propagate, PUIs can undergo a secondary charge exchange with interstellar neutrals, transforming into energetic neutral atoms (ENAs). Observations of these ENAs have been made by missions such as the Interstellar Boundary Explorer (IBEX; D. J. McComas et al. 2009) and Cassini (S. M. Krimigis et al. 2009). Understanding ENAs is crucial because they serve as a means to remotely probe the physics of PUI acceleration in the heliosphere and beyond. Recently, various models have attempted to simulate ENA fluxes at 1 au, considering different acceleration mechanisms of PUIs at the HTS and/or in the IHS to explain ENA observations by IBEX and Cassini (I. I. Baliukin et al. 2020; B. L. Shrestha et al. 2021; E. J. Zirnstein et al. 2021; M. Gkioulidou et al. 2022; M. Kornbleuth et al. 2023; M. Opher et al. 2023; B. Wang et al. 2023). However, their results have generally revealed the energy-dependent discrepancy between observed and simulated ENA fluxes. This suggests that these models currently lack a comprehensive account of all processes involved in PUI heating. All the considered heating mechanisms in those studies occur at the HTS and further at larger distances in the IHS. Following an analysis of New Horizons observations in the supersonic solar wind region, P. A. Isenberg et al. (2023) demonstrated that the cooling of PUIs can differ from the initial predictions made by the V. M. Vasyliunas & G. L. Siscoe (1976) model. Their findings indicate that PUIs experience continuous heating attributed to the presence of ambient turbulence in the outer heliosphere.

Beyond the usual heating of PUIs due to the presence of turbulence, New Horizons observations indicate unusual PUI heating occurring between 2015 and 2020. Most of the previous steady-state models can generally capture the trends of solar wind and PUI temperatures in the outer heliosphere but fail to replicate the observed bump in PUI temperature during this period (L. Adhikari et al. 2023). This suggests the need to also investigate additional heating mechanisms inside the supersonic solar wind region. In this paper, we investigate the causes of the bump in the PUI temperature. First, we analyze observations from New Horizons and 1 au spacecraft, demonstrating the direct correlation between solar wind conditions at 1 au and PUI temperature in the outer heliosphere. For this purpose, we employ a nearly incompressible magnetohydrodynamic turbulence transport model to investigate various solar wind conditions and their impact on PUI temperature. Next, we examine the effect of shocks on PUI heating in the supersonic solar wind. We utilize a PUI-mediated plasma model (G. P. Zank et al. 2014; P. Mostafavi et al. 2017a; G. P. Zank et al. 2018) to describe the structure of outer heliospheric shocks and their influence on PUI heating.

This paper is organized as follows. We first show New Horizons observations over the past decade. In Section 3, we investigate possible reasons for the observed bump in the PUI temperature during the 2015–2020 period. Finally, we summarize our results in Section 4.

2. Observations

The New Horizons spacecraft, launched by NASA in 2006, was primarily designed for the study of Pluto and Kuiper Belt objects (S. A. Stern 2008). Since its launch, it has made significant contributions to the field of planetary science, leading to paradigm-shifting discoveries at Pluto and Arrokoth. New Horizons has gone beyond its original goals, offering many new insights into our heliosphere. New Horizons is now the only spacecraft in the outer heliosphere and its instruments are enabling new discoveries about the outer heliosphere and thus providing much valuable science to the heliophysics

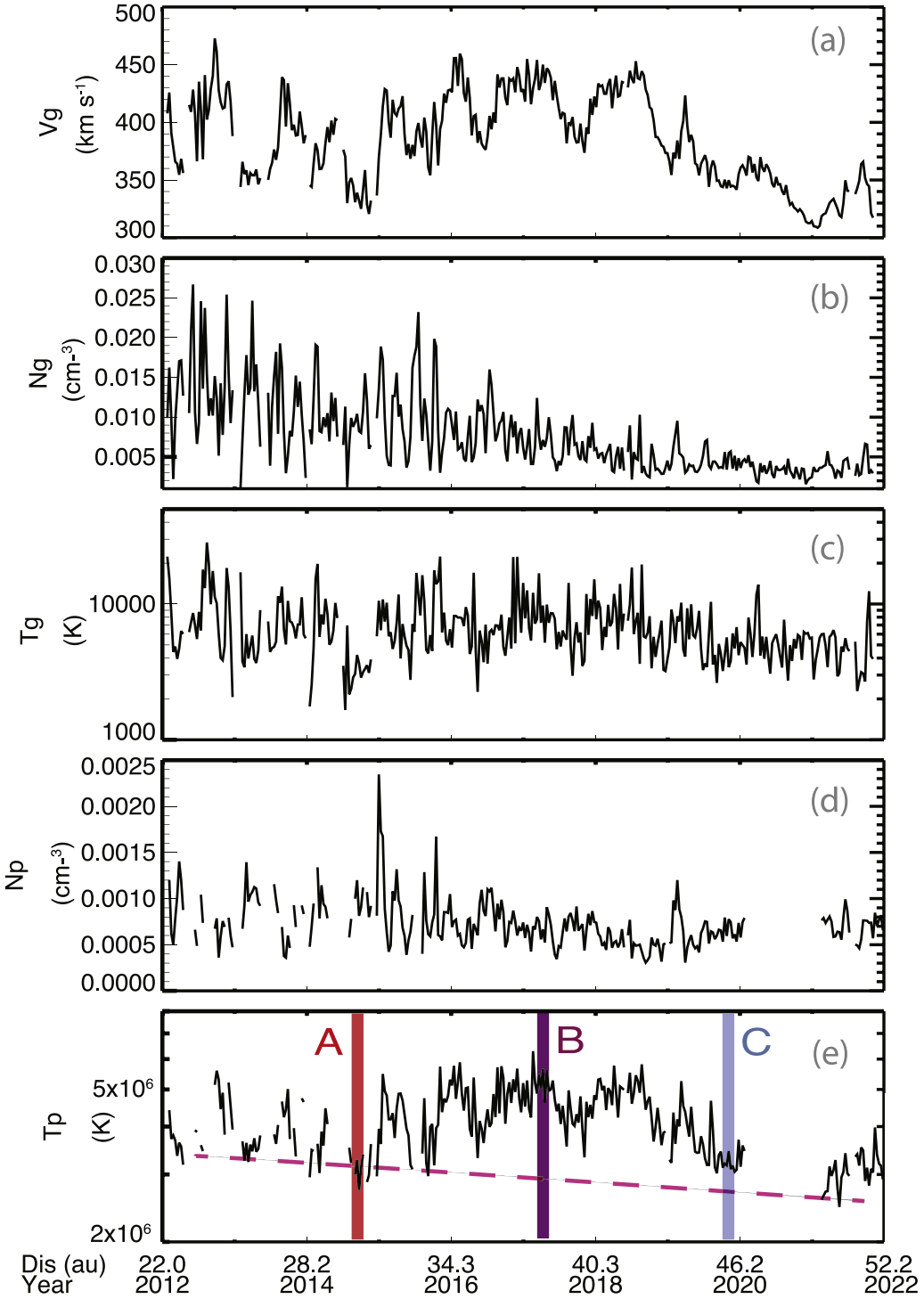

Figure 1. Plots of 5 day averages of thermal solar wind and energetic PUI parameters observed by New Horizons between 2012 and 2022 as the spacecraft traveled from ~22 to 52 au from the Sun. The panels, from top to bottom, display (a) solar wind speed (V_g), (b) solar wind density (N_g), (c) thermal solar wind temperature (T_g), (d) H^+ PUI density (N_p), and (e) nonthermal PUI temperature (T_p). The dashed pink line highlights the observed bump in PUI temperature between 2015 and 2020. Note that PUI data for 2020 are not yet available. The vertical shaded regions mark three different intervals: period A (red; before the PUI temperature enhancement), period B (purple; during the enhancement), and period C (blue; after the enhancement).

community. For instance, SWAP (D. McComas et al. 2008) and PEPSSI (R. L. McNutt et al. 2008; P. Kollmann et al. 2019) instruments on New Horizons are making in situ measurements of H^+ and He^+ PUIs at large distances from the Sun for the first time. In this paper, we focus particularly on studying the thermal solar wind and H^+ PUIs detected by the SWAP instrument. Figure 1 illustrates the radial and temporal evolution of the solar wind and H^+ PUI properties as observed by the SWAP instrument. The panels display 5 day averages of the thermal solar wind speed (panel (a)), density (panel (b)), temperature (panel (c)), nonthermal PUI density (panel (d)), and temperature (panel (e)) over a 10 yr period (2012–2022). This period encompasses most of solar cycle 24 and the beginning of solar cycle 25. The nonthermal PUI temperature

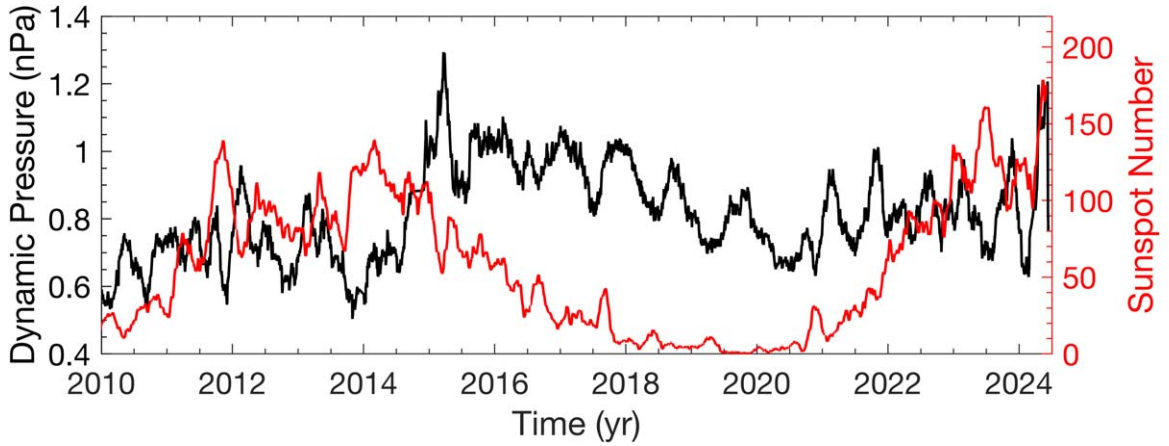

Figure 2. Sunspot number (red) and solar wind dynamic pressure at 1 au (black; $1/2m_pN_gV_g^2$) between 2010 and 2024 (smoothed over two Carrington rotations). An enhancement in solar wind dynamic pressure occurred at the end of 2014, coinciding with the beginning of the declining phase of the solar cycle 24.

exhibits an anomalous rise and subsequent decline between 2015 and 2020, as shown in Figure 1(e). In the next section, we investigate the causes of this extra heating of PUIs.

3. PUI Heating in the Supersonic Solar Wind

Thermal solar wind and suprathermal PUIs can undergo heating through various processes as they propagate in the outer heliosphere. Large-scale turbulence fluctuations cascade energy from large to small scales, where they eventually dissipate to heating plasma. Turbulence is therefore regarded as a promising mechanism for heating the solar wind in the supersonic solar wind (G. P. Zank et al. 1996a, 2017; W. H. Matthaeus et al. 1999; L. Adhikari et al. 2017, 2023; G. Livadiotis 2019). Based on quasi-linear analysis of PUIs in the outer solar wind, guided by New Horizons observations, P. A. Isenberg et al. (2023) theoretically demonstrated that PUIs can experience less cooling than originally predicted by the V. M. Vasyliunas & G. L. Siscoe (1976) model. They proposed that PUIs may undergo continuous heating due to ambient turbulence in the outer heliosphere. New Horizons observations reveal an unusual bump in PUI temperature between approximately 2015 and 2020, which cannot be explained by the heating mechanisms associated with turbulence (see Figure 1(e)). In this work, we suggest two mechanisms as the source of the observed PUI temperature bump.

3.1. Solar Wind Conditions at 1 au

Solar wind dynamic pressure observations at 1 au by the ACE and Wind spacecraft revealed an enhancement of about 50% at the end of 2014 over a short period of time (see Figure 2). D. J. McComas et al. (2017) predicted that changes in the dynamic pressure of the solar wind would significantly impact the outer heliosphere. Later IBEX observations identified the response of the ENA flux to the sudden and dramatic enhancement in the solar wind dynamic pressure (D. J. McComas et al. 2018b, 2020; E. J. Zirnstein et al. 2018a). The IBEX observations revealed that the initial effect was an increase in the population of highest-energy ENAs (at ~4.3 keV), driven by their rapid propagation. This increase was followed by a subsequent rise in relatively lower energy ENAs after a few months/years, albeit with smaller changes in their numbers. Thus, the impact of variable solar wind dynamic pressure on the flux of ENAs at 1 au has been studied extensively in prior research (E. J. Zirnstein et al. 2018a; D. J. McComas et al. 2020). In this study, we investigate the direct influence of the increase in solar wind dynamic pressure on the PUI temperature observed by New Horizons.

We use the turbulence-driven solar wind model of L. Adhikari et al. (2023) to calculate the PUI temperature in the outer heliosphere. The turbulence model was developed based on a nearly incompressible magnetohydrodynamic (NI MHD) phenomenology in a high-plasma-beta regime, which is applicable to the outer heliosphere (G. P. Zank et al. 2017, 2018). The 1D steady-state NI MHD turbulence transport model equations are coupled to a three-fluid (electron, "e," proton, "s," and PUI, "p") solar wind model (Equations (5)–(12)) from 1 to 75 au. The 1D steady-state NI MHD turbulence transport equations in a spherical coordinate system are given by (L. Adhikari et al. 2023)

$$U\frac{d\langle z^{\pm 2}\rangle}{dr}+\left(\frac{dU}{dr}+\frac{2U}{r}\right)\left(\frac{\langle z^{\pm 2}\rangle}{2}+\frac{E_D}{2}\right)=-2\alpha\frac{\langle z^{\pm 2}\rangle\langle z^{\mp 2}\rangle^{1/2}}{\lambda^{\pm}}+2c^{\pm}\frac{r_0\,|\,\Delta U\,|\,V_{A0}^2}{r^2}+\frac{f_D n_H^{\infty}UV_A^{'}\exp\left(\frac{-L}{r}\right)}{n_{sw}^0\,\tau_{ion}^0}, \quad (1)$$

$$U\frac{dE_D}{dr}+\left(\frac{dU}{dr}+\frac{2U}{r}\right)\left(\frac{E_D}{2}+\frac{\langle z^{+2}\rangle+\langle z^{-2}\rangle}{4}\right)=-\alpha E_D\left(\frac{\langle z^{-2}\rangle^{1/2}}{\lambda^{+}}+\frac{\langle z^{+2}\rangle^{1/2}}{\lambda^{-}}\right)+c_{E_D}\frac{r_0\,|\,\Delta U\,|\,V_{A0}^2}{r^2}, \quad (2)$$

$$U\frac{d\lambda^{\pm}}{dr}+\frac{1}{4}\left(\frac{dU}{dr}+\frac{2U}{r}\right)(\lambda_D-2\lambda^{\pm})\frac{E_D}{\langle z^{\pm 2}\rangle}=2\beta^0\langle z^{\mp 2}\rangle^{1/2}-\frac{\lambda^{\pm}}{\langle z^{\pm 2}\rangle}\frac{\beta^0}{\alpha}\left[2c^{\pm}\frac{r_0\,|\,\Delta U\,|\,V_{A0}^2}{r^2}+\frac{f_D n_H^{\infty}UV_A^{'}\exp\left(\frac{-L}{r}\right)}{n_{sw}^0\,\tau_{ion}^0}\right], \quad (3)$$

$$U\frac{d\lambda_D}{dr}-\frac{1}{4E_D}\left(\frac{dU}{dr}+\frac{2U}{r}\right)[(\lambda_D-2\lambda^{+})\langle z^{+2}\rangle+(\lambda_D-2\lambda^{-})\langle z^{-2}\rangle]=\beta^0\lambda_D\left(\frac{\langle z^{-2}\rangle^{1/2}}{\lambda^{+}}+\frac{\langle z^{+2}\rangle^{1/2}}{\lambda^{-}}\right)-c_{E_D}\frac{\beta^0}{\alpha}\frac{\lambda_D}{E_D}\frac{r_0\,|\,\Delta U\,|\,V_{A0}^2}{r^2}, \quad (4)$$

where $\beta^0=\alpha/2$ is the von Kármán Taylor constant which controls the cascade rate of turbulence (W. H. Matthaeus et al. 1996; B. Breech et al. 2008), $\langle z^{\pm 2}\rangle$ denotes the outward/inward Elsässer energy (here we remind the readers that $\langle z^{-2}\rangle\neq\langle 1/z^2\rangle$),

E_D the residual energy, $\lambda^{\pm}$ the correlation length corresponding to $\langle z^{\pm 2}\rangle$, λ_D the correlation length corresponding to E_D, U is the solar wind speed, and $V_A^{'}$ is the (azimuthal) Alfvén velocity. The parameter ΔU is the difference between fast and slow solar wind speeds. We choose $\Delta U = 200\,\mathrm{km\,s^{-1}}$, which is close to the value of C. Larrodera & C. Cid (2020). Furthermore, we assume ΔU to be a constant as we solve for a steady-state model. The parameter V_{A0} is the Alfvén velocity at the reference point r_0(=1 au). The parameters $c^{\pm}$ and c_{E_D} are the parameterized strengths of the turbulent shear source, and f_D is the fraction of the PUI-driven turbulence source that drives turbulence in the outer heliosphere. The parameter $n_H^{\infty} = 0.127\,\mathrm{cm^{-3}}$ is the interstellar neutral hydrogen number density at the HTS (P. Swaczyna et al. 2020), n_{sw}^0 is the solar wind number density at 1 au, $\tau_{ion}^0 = 10^6$ s is the neutral ionization time at 1 au, and $L = 5$ au is the ionization cavity length scale (D. Rucinski & M. Bzowski 1995). It is assumed that the turbulent shear source supplies energy in equal amounts to the outward and inward Elsässer energies ($c^+ \sim c^-$), and differently for the residual energy ($c^{\pm} \neq c_{E_D}$). Note that Equations (1)–(4) are obtained by using the value of structural similarity parameter a (=1/2)n (see G. P. Zank et al. 2012) in the turbulence transport equations of L. Adhikari et al. (2023).

The 1D steady-state solar wind proton and PUI continuity equations as well as the momentum equation can be written as (G. P. Zank et al. 2018)

$$\frac{1}{r^2}\frac{d}{dr}(r^2\rho_s U) = -\nu_c^s \rho_s, \tag{5}$$

$$\frac{1}{r^2}\frac{d}{dr}(r^2\rho_p U) = \nu_c^s \rho_s + \nu_{p0} m_p n_H^{\infty} \exp\left(\frac{-L}{r}\right)\left(\frac{r_0}{r}\right)^2, \tag{6}$$

$$\rho_s U\frac{dU}{dr} + \frac{dP_s}{dr} + \frac{dP_e}{dr} + \frac{dP_p}{dr} + \frac{B}{\mu_0}\frac{dB}{dr} = \nu_{p0} m_p n_H^{\infty} \exp\left(\frac{-L}{r}\right)\left(\frac{r_0}{r}\right)^2 (U_H - U) + (\nu_c^s \rho_s + \nu_c^p \rho_p)(U_H - U), \tag{7}$$

where ρ_s is the solar wind density, ρ_p is the PUI density, m_p is the proton mass, and $U_H = 20\,\mathrm{km\,s^{-1}}$ is the speed of the neutral H. Similarly, P_s, P_e, and P_p represent the solar wind proton pressure, solar wind electron pressure, and PUI pressure, respectively. The symbol B denotes the azimuthal magnetic field. ν_c^s and ν_c^p represent the charge-exchange rates between solar wind protons and interstellar neutral hydrogen, and between PUIs and interstellar neutral hydrogen, respectively, as given by T. E. Holzer (1972),

$$\nu_c^s = \nu_{c0} n_H^{\infty} \exp\left(\frac{-L}{r}\right)\left[\frac{128 k_B}{9\pi m_p}(T_s + T_H) + (\boldsymbol{U} - \boldsymbol{U}_H)^2\right]^{1/2}, \tag{8}$$

$$\nu_c^p = \nu_{c0} n_H^{\infty} \exp\left(\frac{-L}{r}\right)\left[\frac{128 k_B}{9\pi m_p}(T_p + T_H) + (\boldsymbol{U} - \boldsymbol{U}_H)^2\right]^{1/2}, \tag{9}$$

where T_s and T_p denote solar wind and PUI temperature, respectively. $T_H = 6500$ K is the neutral H temperature, $\nu_{c0} = 2 \times 10^{-15}\,\mathrm{cm^2}$ is the charge-exchange cross-section, and k_B is Boltzmann's constant. In Equations (6)–(9), we use $N = n_H^{\infty}\exp(-L/r)$, which is the interstellar neutral hydrogen density, compared with the equations of G. P. Zank et al. (2018). The 1D steady-state transport equation for the P_s, P_e, and P_p can be expressed as

$$U\frac{dP_s}{dr} + \gamma_s P_s\frac{dU}{dr} + 2\gamma_s\frac{U}{r}P_s = (\gamma_s - 1)[\nu_{se}(P_e - P_s) + f_p S_t] - \nu_c^s \rho_s \frac{k_B T_s}{m_p}, \tag{10}$$

$$U\frac{dP_e}{dr} + \gamma_e P_e\frac{dU}{dr} + 2\gamma_e\frac{U}{r}P_e = (\gamma_e - 1)[\nu_{es}(P_s - P_e) - \nabla\cdot\boldsymbol{q}_e + (1 - f_p)S_t], \tag{11}$$

$$U\frac{dP_p}{dr} + \gamma P_p\frac{dU}{dr} + 2\gamma\frac{U}{r}P_p = (\gamma_p - 1)(S_p^{ph} + \nu_c^s\rho_s + \nu_c^p\rho_p)\left(\frac{1}{2}(U_H - U)^2 + \frac{3}{2}\frac{k_B T_H}{m_p}\right) - \nu_c^p \rho_p \frac{k_B T_p}{m_p}, \tag{12}$$

where ν_{se} denotes the collisional frequency between solar wind protons and electrons (G. P. Zank 2014; P. Mostafavi & G. P. Zank 2018; L. Adhikari et al. 2023). We assume that $\nu_{se} \sim \nu_{es}$ (S. R. Cranmer et al. 2009). The heat flux, q, is assumed to be given by the empirical formula (S. R. Cranmer et al. 2009)

$$\ln\left(\frac{q_{\|,e}}{q_0}\right) = -0.7037 - 2.115x - 0.2545x^2, \tag{13}$$

where $x \equiv \ln(r/1\,\mathrm{au})$ and $q_0 = 0.01\,\mathrm{erg\,cm^{-2}\,s^{-1}}$.

For our analysis, we selected three specific periods from the New Horizons observations: before (period A), during (period B), and after (period C) the PUI temperature enhancement (see Figure 1(e)). We then backtrack the solar wind speed (averaged over one Carrington rotation) during these three periods to 1 au. One Carrington averaging of the selected periods was employed to minimize the impact of point-to-point variations in the solar wind speed observed by SWAP. The slowing of the solar wind by mass-loading effect is accounted for by using a first-order approximation of a 5% change in the solar wind speed, based on recent comparisons of New Horizons and 1 au observations (see H. A. Elliott et al. 2019, for more details). The solar wind conditions at 1 au from OMNI data during these periods are used as the boundary conditions for our simulation (see Table 1). The parameter values used in the model for the three cases are shown in Table 2.

Figure 3 presents the PUI temperature observed by New Horizons (gray dots) alongside simulation results derived from the propagation of PUIs for the three selected intervals (solid curves). This figure clearly illustrates that interval B (purple curve at the marked X position), characterized by higher solar wind speeds and dynamic pressure at 1 au, generates hotter PUIs compared to intervals A (red curve) and C (cyan curve) at their marked X positions. The results show that PUIs generated from the charge exchange of interstellar neutral atoms with faster solar winds are initially hotter upon formation. Consequently, the bump observed in PUI temperature by New Horizons is primarily associated with the enhanced solar wind dynamic pressure previously observed at 1 au.

Table 1
Boundary Values for the Solar Wind, PUI, and the Turbulence Quantities at 1 au for the Three Cases A, B, and C Shown in Figure 1

Quantities	A	B	C
$\langle z^{+2}\rangle$ (km^2 s^{-2})	1486.25	1818.39	841.51
$\langle z^{-2}\rangle$ (km^2 s^{-2})	520.77	483.78	324.98
E_D (km^2 s^{-2})	−300.5	−285.39	−161.59
λ^+ (km)	5.7×10^5	5.7×10^5	5.4×10^5
λ^- (km)	4.2×10^5	3.6×10^5	3.6×10^5
λ_D (km)	1.4×10^6	1.69×10^6	1.27×10^6
U (km s^{-1})	400	475	387
n_s (cm^{-3})	6.8	10	5.72
n_p (cm^{-3})	5.05×10^{-6}	6.06×10^{-6}	4.04×10^{-6}
P_s (Pa)	6.99×10^{-12}	1.31×10^{-11}	5.15×10^{-12}
P_e (Pa)	3.49×10^{-12}	6.53×10^{-12}	2.57×10^{-12}
P_p (Pa)	5.78×10^{-23}	6.93×10^{-23}	4.62×10^{-23}

Table 2
Values of the Parameters Used for the Three Cases A, B, and C

Parameters	A	B	C
α	0.03	0.03	0.03
β^0	0.015	0.015	0.015
f_D	0.04	0.04	0.04
c^+	0.3	0.3	0.3
c^-	0.3	0.3	0.3
c_{E_D}	−0.05	−0.05	−0.05
V_{A0} (km s^{-1})	54.66	51.72	39.01
ΔU (km s^{-1})	200	200	200

3.2. Shock Waves

Shock waves originating from coronal mass ejections (CMEs) and corotating interaction regions (CIRs; L. A. Fisk & M. A. Lee 1980; G. P. Zank et al. 1996b; K. Tsubouchi 2017; E. J. Zirnstein et al. 2018b) propagate into the outer heliosphere. CIRs occur when fast solar wind streams from coronal holes overtake slower solar wind, as reviewed by I. G. Richardson (2018). This interaction results in a region of compressed plasma and the formation of shocks, both forward and reverse, at the leading and trailing edges of the CIR beyond 1 au (E. J. Smith & J. H. Wolfe 1976; I. G. Richardson 2018). CIRs are especially notable features of the solar wind during the declining and minimum phases of the 11 yr solar cycle (I. G. Richardson 2006; I. G. Richardson & H. V. Cane 2012). However, CMEs and the associated shocks tend to have the highest occurrence frequencies during solar maximum (D. F. Webb & R. A. Howard 1994). Even though shocks associated with CIRs are typically weaker than CME shocks, they are very frequent and have a cycle of approximately every 27 days, especially during the declining phase of the solar cycle (I. G. Richardson 2018).

The other important mechanism capable of heating and accelerating PUIs is interplanetary shocks in the outer heliosphere. Previous studies have shown that as the PUI pressure becomes the dominant pressure (L. F. Burlaga et al. 1996; D. J. McComas et al. 2017) in the outer heliosphere beyond 10 au, PUIs experience preferential heating at outer heliospheric shocks such as CIRs (G. Gloeckler et al. 1994; G. P. Zank et al. 1996b; G. Gloeckler & J. Geiss 1998; E. J. Zirnstein et al. 2018b; D. J. McComas et al. 2021; B. L. Shrestha et al. 2023), the HTS (G. P. Zank et al. 1996b, 2010; P. Mostafavi et al. 2017a, 2018; R. Kumar et al. 2018; B. Lembége et al. 2020) and shocks in the IHS (P. Mostafavi et al. 2019). Recently, D. J. McComas et al. (2022) analyzed New Horizons observations and showed that shocks in the outer heliosphere are PUI-mediated shocks and core solar wind density and temperature do not show significant changes across these shocks. They have also demonstrated that the shocks in the distant outer heliosphere are much wider than shocks observed at 1 au.

As demonstrated in Section 3.1, the overall trend of PUI temperature follows the solar wind speed. However, the comparison between the curves in Figure 3 and the maximum PUI temperature observed by SWAP shows that there are additional occasional enhancements in the PUI temperature that necessitate consideration of other mechanisms responsible for heating these particles during those times. The enhancement in PUI temperature observed by New Horizons occurred during the declining phase of the solar cycle, as indicated by the sunspot numbers shown by the red curve in Figure 2. During this phase, CIR shocks are a common feature, and New Horizons observations documented the frequency of CIR shocks in the outer heliosphere during this period (e.g., see Figure 6 of D. J. McComas et al. 2021). These shocks can be partly responsible for some of the PUI heating. P. Mostafavi et al. (2018, 2019) showed that the HTS and shocks in the IHS preferentially heat the PUIs, while the thermal gas usually behaves adiabatically. Here, we use our two-fluid model to investigate the PUI and solar wind heating associated with shocks in the supersonic solar wind before reaching the HTS.

PUIs in the supersonic solar wind beyond 10 au are not equilibrated with the background thermal plasma and should be treated as a separate component (G. P. Zank et al. 2014). We utilize a two-fluid (thermal solar wind and H^+ PUI) model, the PUI-mediated plasma model, as presented by P. Mostafavi et al. (2017a) and P. Mostafavi et al. (2019), to simulate shocks in the outer heliosphere. PUIs undergo pitch-angle scattering, generating dissipation terms such as collisionless heat flux and collisionless viscosity in the system (see G. P. Zank et al. 2014, for more details).

Due to the Parker spiral structure of the magnetic field in the outer heliosphere, the majority of shocks encountered in this region tend to be quasi-perpendicular. The structure of a steady PUI-mediated perpendicular shock is governed by (details given in P. Mostafavi et al. 2018, 2019)

$$\frac{d^2y}{dx'^2}+\frac{3}{\mathrm{Sch}_p}\left[\left(\frac{1}{M_{s1}^2}\left(\frac{1}{y}\right)^{\gamma_p+1}-1\right)-\mathrm{Sch}_p y+\frac{y_B}{y^3}\right]\frac{dy}{dx'}=\frac{9}{\mathrm{Sch}_p}\frac{\gamma_p}{\gamma_g M_{s1}^2}(1-y)Z(y), \tag{14}$$

where

$$Z(y)\equiv\gamma_g M_{s1}^2\frac{\gamma_p+1}{2}\left(y-\frac{\gamma_p-1}{\gamma_p+1}\right)-1+\frac{P_{p1}}{P_{g1}}-\frac{(\gamma_g-\gamma_p)}{\gamma_p(\gamma_g-1)}\frac{(1-y^{1-\gamma_g})}{(1-y)}-\gamma_g M_{s1}^2\frac{y_B}{2y}\left(\frac{\gamma_p-2}{\gamma_p}-y\right). \tag{15}$$

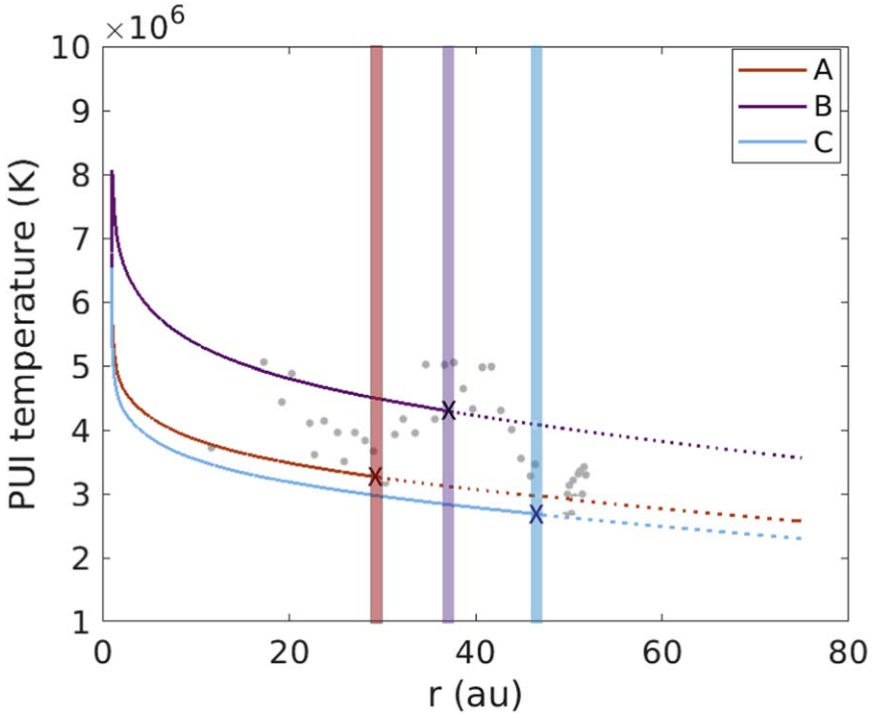

Figure 3. Comparison of the theoretical PUI temperature (solid curves) with the measured PUI temperature (gray dots) of New Horizons SWAP as a function of distance. The theoretical results are calculated for three cases (A, B, and C; see vertical lines) using three boundary conditions shown in Table 1. The X points represent the simulation results for these three cases, which can be compared to the New Horizons observations (gray dots) at the corresponding locations.

Here, y is the inverse compression ratio, and $M_{s1} = \sqrt{\rho_1 U_1/\gamma_g P_{g1}}$ is the thermal gas Mach number at the upstream of the shock, ρ is the number density, $\gamma_{g/p}$ is the thermal gas/PUI adiabatic index, and U is the bulk flow velocity. $P_{g1/p1}$ is the thermal gas/PUI pressure far upstream of the shock. $\mathrm{Sch}_p = \eta_p/\rho_1 K_p$ is the PUI Schmidt number, which is the ratio between PUI collisionless viscosity $\eta_p \sim P_p \tau_s$ and PUI heat flux $K_p = \frac{1}{3}\tau_s U_1^2 \frac{B^2}{\langle \delta B^2 \rangle}$. x' is the distance normalized to the PUI diffusion length scale K_p/U and y_B is the square of the inverse Alfvén Mach number. The PUI pitch-angle scattering timescale, τ_s, in the outer heliosphere at approximately 35 au is calculated to be ~199.1 s, resulting in a PUI viscosity coefficient of 7.9×10^{-12} kg m^{-1} s^{-1} (see G. P. Zank 2014, for more details about the equations). Thus, the PUI Schmidt number for this distance and the assumed quantities is about 0.08. Since New Horizons does not have a magnetometer, we use an estimated magnetic field strength at this distance of about 0.105 nT (L. Adhikari et al. 2023) in our calculations.

All the mentioned quantities have been used in Equations (14) and (15) to simulate a perpendicular shock in the supersonic region of the outer heliosphere (e.g., a shock located at 35 au from the Sun). New Horizons observations show that the suprathermal PUIs at this distance have a number density of about 10% of the thermal solar wind ion density, and they contribute a significantly larger pressure compared to the thermal plasma, $P_p/P_g \sim 60$. We use a thermal solar wind density of 0.005 cm^{-3} and adiabatic index of $\gamma_p = \gamma_g = 5/3$.

Figure 4 shows the results of the simulated shock with $M_{s1} = 13$ and $y_B = 0.1$. Figure 4 shows that the shock has a weak smooth transition with a compression ratio of 1.9. The normalized thermal gas (blue curve), magnetic (green curve), and PUI (red curve) pressures as a function of normalized distance are plotted in Figure 4(b). This shows that PUI pressure is the dominant component upstream and downstream of the shocks in the outer heliosphere. As observed at the HTS (P. Mostafavi et al. 2017b) and shocks in the IHS (P. Mostafavi et al. 2019), the thermal gas does not contribute significantly to the downstream pressure. Therefore, even weak outer heliospheric shocks are mediated by suprathermal PUIs. Recent analysis of New Horizons data by D. J. McComas et al. (2022) revealed that shocks in the outer heliosphere are mediated by PUIs, with core solar wind properties remaining largely unchanged across these shocks. Earlier, Voyager 2 observations also indicated that only a few shocks in this region cause simultaneous jumps in all thermal solar wind parameters, with density changes showing less correlation (A. J. Lazarus et al. 1999).

The thermal gas Mach number through the shock (blue curve in Figure 4(c)) shows that the flow remains supersonic with respect to the thermal gas downstream of the shock. This is a consequence of the thermal gas not gaining much energy and remaining cold through the shock. The very small increase in thermal gas temperature did not correspond to a transition from a supersonic to a subsonic flow. However, the red curve in Figure 4(c) shows the combined thermal gas and PUI Mach number through the shock (sound speed $= \sqrt{a_g^2 + a_p^2}$; see G. P. Zank et al. 2014, for more details). Since PUIs are almost exclusively heated, the transition from upstream to downstream does result in a supersonic to subsonic flow transition. The supersonic thermal gas flow downstream of the shocks has been observed at the New Horizons observations as well (D. J. McComas et al. 2022). As shown in the panels of Figure 4 and the black arrow specifically, the thickness of this shock is normalized by the PUI diffusion length scale (K_p/U) and is approximately 3.5 x' or 0.05 au for this shock. This value is comparable to the shock thicknesses observed by New

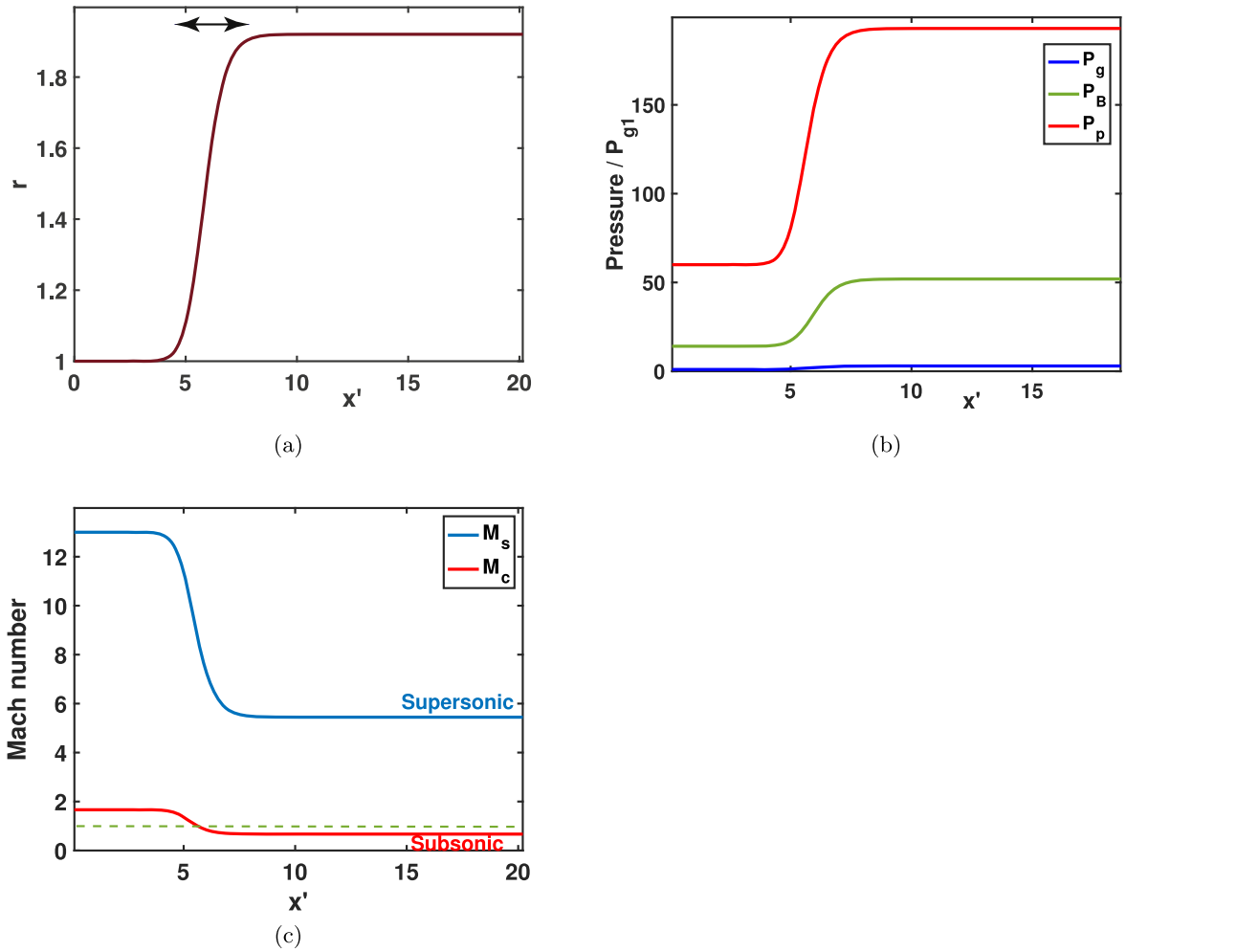

Figure 4. Smoothed shock transition corresponding to a perpendicular shock in the outer heliosphere when PUI dissipation terms (i.e., viscosity and heat flux) are present. (a): compression ratio across the shock. (b): thermal gas (blue), magnetic (green), and PUI (red) pressures normalized to the thermal gas pressure far upstream of the shock. This shows that the shock is mediated by energetic PUIs, with almost all the upstream ram energy being converted to downstream PUI internal energy. (c): the thermal gas Mach number, $M_s = u/a_g$, and combined thermal gas and PUI Mach number, $M_c = u/\sqrt{a_g^2 + a_p^2}$, through the shock. The green dashed line specifies the Mach number equals to one. The flow is subsonic downstream of the shock only if the combined sound speed, including PUIs, is used (red curve). The black arrow in (a) indicates the shock thickness from upstream to downstream, which is then converted to an unnormalized value of 0.05 au.

Horizons (D. J. McComas et al. 2022). This broader thickness, compared to inner heliospheric shocks, is due to the large diffusion coefficient associated with energetic PUIs. Similar to the HTS (P. Mostafavi et al. 2017a), shocks in the outer heliosphere are mediated by PUIs and thus broad for this reason.

Our results confirm that shocks in the outer heliosphere preferentially heat PUIs by a significant amount. The presence of shocks and compression regions in the supersonic solar wind leads to further heating of PUIs and, consequently, more effective production of higher energy ENAs. Therefore, models should incorporate shocks in the supersonic region by using the time-dependent data-driven boundary conditions and account for the additional heating of PUIs by these shocks as was done by some models such as (T. K. Kim et al. 2017). Including shocks can increase the ENA flux, potentially resulting in a better alignment with IBEX observations.

4. Summary

Even though Voyager 1 and 2 have provided invaluable data about the outer heliosphere and its intriguing dynamics, New Horizons for the first time is making in situ measurements of the PUIs, which are the essential component in this region. This study examines two possible heating mechanisms for non-thermal energetic PUIs in the outer heliosphere, emphasizing the role of solar wind conditions and shock waves. New Horizons' SWAP instrument detected unexpected PUI heating between 2015 and 2020, as indicated by a notable bump in PUI temperature. Our analysis of New Horizons' SWAP observations, combined with concurrent data from ACE and Wind spacecraft, reveals significant insights into PUI dynamics during those periods. Our simulation results indicate that the observed peak by New Horizons in PUI temperature correlates strongly with an approximately 50% increase in solar wind dynamic pressure at 1 au observed at the end of 2014. Higher solar wind speeds result in the creation of hotter PUIs, which propagate through the heliosphere. When the solar wind speed increases, it not only accelerates the thermal ions in the solar wind but also enhances the interaction between these ions and interstellar neutral atoms. This interaction leads to a more efficient charge-exchange process, resulting in the creation of PUIs with higher initial energies. Consequently, these hotter PUIs retain their energy as they travel outward from the Sun,

contributing to the observed rise in PUI temperature at greater heliocentric distances. This finding suggests that variations in solar wind conditions from the Sun can have far-reaching effects on the properties of PUIs in the distant heliosphere.

Furthermore, the enhancement in the PUI temperature occurred during the declining phase of the solar cycle, which is particularly notable for the frequent occurrence of CIR shocks. Our PUI-mediated plasma model simulations reveal that shocks in the outer heliosphere predominantly heat PUIs, with these shocks being broad due to the high diffusion coefficient of PUIs. These results explain observations of shock structure and preferential PUI heating made by New Horizons. The thermal gas remains supersonic through the shocks without the inclusion of PUIs. This finding highlights the minimal impact of these shocks on the thermal gas compared to their significant effect on PUIs, demonstrating that PUIs are the primary drivers of energy absorption in these regions. These results are very important and help clarify the basic shock physics associated with energetic PUIs. This has general implications for our understanding of the HTS and shocks in the IHS since PUI pressure dominates in these regions.

In conclusion, this study enhances our understanding of the dynamic processes in the outer heliosphere and the critical role of PUIs. The findings highlight that PUIs are significantly influenced by solar wind conditions and interplanetary shocks, leading to their heating and increased production of ENAs. Each of the heating processes discussed here has the potential to further accelerate PUIs within the supersonic region, IHS, and at the HTS. Future models in this field need to incorporate these additional physical processes to better capture the intricate physics governing the heating and acceleration of PUIs. For example, future global MHD models that incorporate PUIs and their evolution in the supersonic solar wind should incorporate the heating by shocks and CIRs as examined here. This comprehensive approach to modeling will not only advance our fundamental understanding of these phenomena but will also provide us with more accurate tools for interpreting observational data. These model enhancements will be especially critical for analyzing data from the upcoming Interstellar Mapping and Acceleration Probe mission (D. J. McComas et al. 2018a) and a future Interstellar Probe mission (P. C. Brandt et al. 2023).

Acknowledgments

The New Horizons work was supported by NASA New Horizons funding through contract NAS5-97271/Task order 30. This work was supported by the NASA Drive Science Centers initiative, under contract 80NSSC20K0603-18-DRIVE18-2-0029 in BU SHIELD DRIVE Science Center. B.L.S. acknowledges the support of the SWAP instrument effort on the New Horizons (M99023MJM; PU-AWD1006357) and IBEX mission (80NSSC20K0719) as part of NASA's Explorer Program. G.P.Z. and L.A. acknowledge the partial support of a Parker Solar Probe contract SV4-84017, an NSF EPSCoR RII-Track-1 cooperative agreement OIA-2148653, and NASA awards 80NSSC20K1783 and 80NSSC21K1319, and NASA Heliospheric Shield award 80NSSC22M0164, BU SAP No. 50210276.

ORCID iDs

Parisa Mostafavi https://orcid.org/0000-0002-3808-3580
Laxman Adhikari https://orcid.org/0000-0003-1549-5256
Bishwas L. Shrestha https://orcid.org/0000-0002-5247-4107
Gary P. Zank https://orcid.org/0000-0002-4642-6192
Merav Opher https://orcid.org/0000-0002-8767-8273
Matthew E. Hill https://orcid.org/0000-0002-5674-4936
Heather A. Elliott https://orcid.org/0000-0003-2297-3922
Pontus C. Brandt https://orcid.org/0000-0002-4644-0306
Ralph L. McNutt https://orcid.org/0000-0002-4722-9166
David J. McComas https://orcid.org/0000-0001-6160-1158
Andrew R. Poppe https://orcid.org/0000-0001-8137-8176
Elena Provornikova https://orcid.org/0000-0001-8875-7478
Romina Nikoukar https://orcid.org/0000-0002-8608-2822
Peter Kollmann https://orcid.org/0000-0002-4274-9760
S. Alan Stern https://orcid.org/0000-0001-5018-7537
Kelsi N. Singer https://orcid.org/0000-0003-3045-8445
Anne Verbiscer https://orcid.org/0000-0002-3323-9304
Joel Parker https://orcid.org/0000-0002-3672-0603

References

Adhikari, L., Zank, G. P., Hunana, P., et al. 2017, ApJ, 841, 85
Adhikari, L., Zank, G. P., & Zhao, L. 2021, Fluid, 6, 368
Adhikari, L., Zank, G. P., Wang, B., et al. 2023, ApJ, 953, 44
Axford, W. I. 1972, NASSP, 308, 609
Baliukin, I. I., Izmodenov, V. V., & Alexashov, D. B. 2020, MNRAS, 499, 441
Brandt, P. C., Provornikova, E., Bale, S. D., et al. 2023, SSRv, 219, 18
Breech, B., Matthaeus, W. H., Minnie, J., et al. 2008, JGRA, 113, A08105
Burlaga, L. F., Ness, N. F., Belcher, J. W., & Whang, Y. C. 1996, JGRA, 101, 15523
Cranmer, S. R., Matthaeus, W. H., Breech, B. A., & Kasper, J. C. 2009, ApJ, 702, 1604
Drake, J. F., Opher, M., Swisdak, M., & Chamoun, J. N. 2010, ApJ, 709, 963
Elliott, H. A., McComas, D. J., Zirnstein, E. J., et al. 2019, ApJ, 885, 156
Fisk, L. A., & Gloeckler, G. 2017, JPhCS, 900, 012006
Fisk, L. A., & Lee, M. A. 1980, ApJ, 237, 620
Florinski, V., Zank, G. P., & Pogorelov, N. V. 2005, JGRA, 110, A07104
Giacalone, J., Nakanotani, M., Zank, G. P., et al. 2021, ApJ, 911, 27
Gkioulidou, M., Opher, M., Kornbleuth, M., et al. 2022, ApJL, 931, L21
Gloeckler, G., & Geiss, J. 1998, SSRv, 86, 127
Gloeckler, G., Geiss, J., Balsiger, H., et al. 1993, Sci, 261, 70
Gloeckler, G., Jokipii, J. R., Giacalone, J., & Geiss, J. 1994, GeoRL, 21, 1565
Hollick, S. J., Smith, C. W., Pine, Z. B., et al. 2018a, ApJ, 863, 75
Hollick, S. J., Smith, C. W., Pine, Z. B., et al. 2018b, ApJS, 237, 34
Holzer, T. E. 1972, JGR, 77, 5407
Isenberg, P. A., Vasquez, B. J., & Smith, C. W. 2023, ApJ, 944, 84
Kim, T. K., Pogorelov, N. V., & Burlaga, L. F. 2017, ApJL, 843, L32
Kollmann, P., Hill, M. E., McNutt, R. L., et al. 2019, ApJ, 876, 46
Kornbleuth, M., Opher, M., Zank, G. P., et al. 2023, ApJL, 944, L47
Krimigis, S. M., Mitchell, D. G., Roelof, E. C., Hsieh, K. C., & McComas, D. J. 2009, Sci, 326, 971
Kumar, R., Zirnstein, E. J., & Spitkovsky, A. 2018, ApJ, 860, 156
Larrodera, C., & Cid, C. 2020, A&A, 635, A44
Lazarus, A. J., Richardson, J. D., Decker, R. B., & McDonald, F. B. 1999, in AIP Conf. Proc. 471, The solar wind nine conference, ed. S. R. Habbal et al. (Melville, NY: AIP), 771
Lembége, B., Yang, Z., & Zank, G. P. 2020, ApJ, 890, 48
Livadiotis, G. 2019, ApJ, 887, 117
Matthaeus, W. H., Zank, G. P., & Oughton, S. 1996, JPlPh, 56, 659
Matthaeus, W. H., Zank, G. P., Smith, C. W., & Oughton, S. 1999, PhRvL, 82, 3444
McComas, D., Allegrini, F., Bagenal, F., et al. 2008, SSRv, 140, 261
McComas, D. J., Allegrini, F., Bochsler, P., et al. 2009, Sci, 326, 959
McComas, D. J., Bzowski, M., Dayeh, M. A., et al. 2020, ApJS, 248, 26
McComas, D. J., Christian, E. R., Schwadron, N. A., et al. 2018a, SSRv, 214, 116
McComas, D. J., Dayeh, M. A., Funsten, H. O., et al. 2018b, ApJL, 856, L10
McComas, D. J., Shrestha, B. L., Swaczyna, P., et al. 2022, ApJ, 934, 147
McComas, D. J., Swaczyna, P., Szalay, J. R., et al. 2021, ApJS, 254, 19
McComas, D. J., Zirnstein, E. J., Bzowski, M., et al. 2017, ApJS, 233, 8
McNutt, R. L., Livi, S. A., Gurnee, R. S., et al. 2008, SSRv, 140, 315
Mostafavi, P., & Zank, G. P. 2018, ApJL, 854, L15
Mostafavi, P., Zank, G. P., & Webb, G. M. 2017a, ApJ, 841, 4
Mostafavi, P., Zank, G. P., & Webb, G. M. 2017b, JPhCS, 900, 012016
Mostafavi, P., Zank, G. P., & Webb, G. M. 2018, ApJ, 868, 120

Mostafavi, P., Zank, G. P., Zirnstein, E. J., & McComas, D. J. 2019, ApJL, 878, L24
Opher, M., Drake, J. F., Swisdak, M., et al. 2011, ApJ, 734, 71
Opher, M., Drake, J. F., Zank, G., et al. 2021, ApJ, 922, 181
Opher, M., Drake, J. F., Zieger, B., & Gombosi, T. I. 2015, ApJL, 800, L28
Opher, M., Richardson, J., Zank, G., et al. 2023, FrASS, 10, 1143909
Richardson, I. G. 2006, Recurrent Magnetic Storms: Corotating Solar Wind Streams (Washington, DC: American Geophysical Union), 45
Richardson, I. G. 2018, LRSP, 15, 1
Richardson, I. G., & Cane, H. V. 2012, JSWSC, 2, A01
Richardson, J. D. 2008, GeoRL, 35, L23104
Richardson, J. D., Burlaga, L. F., Elliott, H., et al. 2022, SSRv, 218, 35
Rucinski, D., & Bzowski, M. 1995, A&A, 296, 248
Semar, C. L. 1970, JGR, 75, 6892
Shrestha, B. L., Zirnstein, E. J., Heerikhuisen, J., & Zank, G. P. 2021, ApJS, 254, 32
Shrestha, B. L., Zirnstein, E. J., McComas, D. J., et al. 2023, ApJ, 960, 35
Siscoe, G. L., & Mukherjee, N. R. 1972, JGR, 77, 6042
Smith, E. J., & Wolfe, J. H. 1976, GeoRL, 3, 137
Sokół, J. M., Kubiak, M. A., & Bzowski, M. 2019, ApJ, 879, 24
Sokół, J. M., Kucharek, H., Baliukin, I. I., et al. 2022, SSRv, 218, 18
Stern, S. A. 2008, SSRv, 140, 3
Swaczyna, P., McComas, D. J., Zirnstein, E. J., et al. 2020, ApJ, 903, 48
Tsubouchi, K. 2017, JGRA, 122, 3935
Vasyliunas, V. M., & Siscoe, G. L. 1976, JGR, 81, 1247
Wang, B., Zhao, L., Abouhamzeh, P., Zank, G. P., & Adhikari, L. 2023, FrASS, 10, 1298577
Webb, D. F., & Howard, R. A. 1994, JGR, 99, 4201
Zank, G. P. 1999, SSRv, 89, 413
Zank, G. P. 2014, Transport Processes in Space Physics and Astrophysics (New York: Springer)
Zank, G. P., Adhikari, L., Zhao, L. L., et al. 2018, ApJ, 869, 23
Zank, G. P., Dosch, A., Hunana, P., et al. 2012, ApJ, 745, 35
Zank, G. P., Du, S., & Hunana, P. 2017, ApJ, 842, 114
Zank, G. P., Heerikhuisen, J., Pogorelov, N. V., Burrows, R., & McComas, D. 2010, ApJ, 708, 1092
Zank, G. P., Hunana, P., & Mostafavi, P. 2015, JPhCS, 577, 012025
Zank, G. P., Hunana, P., Mostafavi, P., & Goldstein, M. L. 2014, ApJ, 797, 87
Zank, G. P., Matthaeus, W. H., & Smith, C. W. 1996a, JGR, 101, 17093
Zank, G. P., Nakanotani, M., Zhao, L. L., et al. 2021, ApJ, 913, 127
Zank, G. P., Pauls, H. L., Cairns, I. H., & Webb, G. M. 1996b, JGR, 101, 457
Zhao, L. L., Zank, G. P., Hu, Q., et al. 2019, ApJ, 886, 144
Zieger, B., Opher, M., Tóth, G., Decker, R. B., & Richardson, J. D. 2015, JGRA, 120, 7130
Zieger, B., Opher, M., Tóth, G., & Florinski, V. 2020, JGRA, 125, e28393
Zirnstein, E. J., Heerikhuisen, J., McComas, D. J., et al. 2018a, ApJ, 859, 104
Zirnstein, E. J., Kumar, R., Bandyopadhyay, R., et al. 2021, ApJL, 916, L21
Zirnstein, E. J., McComas, D. J., Kumar, R., et al. 2018b, PhRvL, 121, 075102